

# ROLE OF THE HOGGAR MASSIF ON THE WEST AFRICAN MONSOON ONSET

Philippe Drobinski <sup>1</sup>, Benjamin Sultan <sup>2</sup>, Serge Janicot <sup>2</sup>

<sup>1</sup> IPSL/SA, BP102, Université Pierre et Marie Curie, 4 place Jussieu, 75252 Paris Cédex 05, France

<sup>2</sup> IPSL/LOCEAN, BP100, Université Pierre et Marie Curie, 4 place Jussieu, 75252 Paris Cédex 05, France

E-mail: [philippe.drobinski@aero.jussieu.fr](mailto:philippe.drobinski@aero.jussieu.fr)

**Abstract:** It has been observed that the West African monsoon onset is concomitant with the enhancement of the Saharan heat low. We show here through a combined diagnostic and modeling study a possible interaction between northern Africa orography and the deepening of the Saharan heat low at the time of the monsoon onset. The amplification of an anticyclonic circulation above and north of the Hoggar massif leads to an increase and a southeasterly-northeasterly rotation of the wind ahead of the Hoggar which contribute to an increased leeward-trough effect enhancing the Saharan heat low. The Atlas does not play any role during the monsoon onset but contributes to the mean climatological location of the Saharan heat low.

**Keywords** – *West African monsoon, heat low, Hoggar massif*

## 1. INTRODUCTION

The onset of the summer monsoon over West Africa is linked to an abrupt latitudinal shift of the Inter-Tropical Convergence Zone (ITCZ) from a quasi-stationary location at 5°N in May-June to another quasi-stationary location at 10°N in July-August (Sultan and Janicot 2003). On the last 35 years, the mean date for the onset occurrence has been 24 June and its standard deviation 8 days. This abrupt shift occurs mostly between 10°W and 5°E where a meridional land-sea contrast exists and it is characterized by a temporary rainfall and convection decrease over West Africa. Sultan and Janicot (2003) suggested that this abrupt ITCZ shift is associated with the low and mid levels atmospheric dynamics of the Saharan heat low located between 15°N and 20°N. The heat low meridional circulation intensity is the highest at the beginning of the monsoon onset, leading both to increase convective inhibition in the ITCZ through intrusion of dry and subsiding air from the north, and to increase potential instability through a greater inland moisture advection and a higher monsoon depth induced by a stronger cyclonic circulation in the low-levels. During the monsoon onset, once the rainfall minimum occurred due to the convective inhibition, the accumulated potential instability breaks the convective inhibition, the inertial instability of the monsoon circulation is released and the associated regional scale circulation increases, leading to the abrupt shift of the ITCZ. Then the ITCZ moves to the north up to 10°N, where thermodynamical conditions are favorable. Sultan and Janicot (2003) suggested that the amplification of the heat low dynamics, associated with the abrupt monsoon onset, could be due to an interaction with the northern orography of the Atlas-Hoggar mountains. The aim of this paper is to investigate this orography-induced forcing on the heat low dynamics at the time of the West African monsoon onset by using the results of the composite approach described by Sultan and Janicot (2003) applied to the NCEP-NCAR atmospheric reanalyses. Results will be compared with simulations of a linear model describing the atmospheric circulation anomalies in response to orography.

## 2. THE COMPOSITE APPROACH

Sultan and Janicot (2003) applied a quasi-objective method to define a date of the monsoon onset by using daily gridded rainfall data from the NCAR-NCEP reanalyses over the period 1968-1990, and then used these dates, called  $t_0$ , as a respective reference date for each year to define the composite mean atmospheric patterns which might control the abrupt shift of the ITCZ around  $t_0$ . Figure 1 shows such a result for the composite mean sea level pressure and 1000 hPa wind fields at  $t_0$  minus 5 days,  $t_0$  plus 5 days, and the difference between  $t_0+5$  and  $t_0-5$ . Shaded areas depict the orography of northern Africa with the Atlas mountains centered at 5°W-32.5°N, the Hoggar mountains centered at 7.5°E-25°N, the Tibesti mountains at 17.5°E-20°N, and a group of three mountains called here Ennedi at 23°E-15°N.

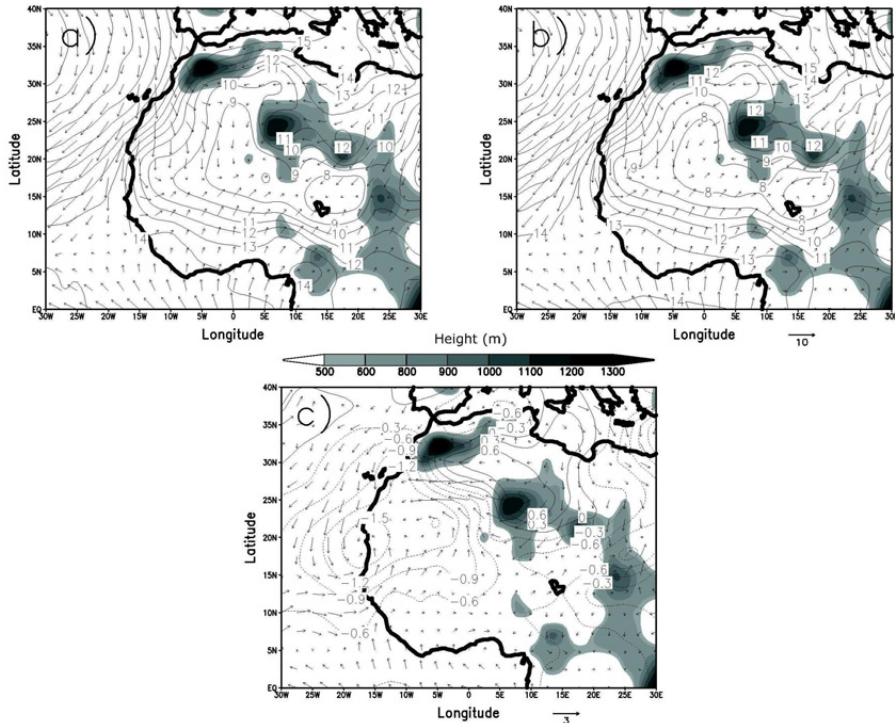


**Figure 1.** (a) Composite NCEP/NCAR mean sea level pressure and 1000 hPa wind field (vector scale ( $m s^{-1}$ ) is displayed below) at  $t_0-5$  averaged over the period 1968-1990 by using as the reference date  $t_0$  the ITCZ shift date for each year. Mean sea level pressure is expressed in hPa where the 1000 hPa value is subtracted. Shaded areas depict the orography of northern Africa (m; areas higher than 400 meters are shaded by step of 100 m). (b) Same as (a) but for  $t_0+5$ . (c) Difference between (b) and (a).

At  $t_0-5$  (Fig. 1a), the axis of low pressures of the Saharan heat low follow the southern border of the northern African orography in a southeast-northwest crescent-shaped, with a high pressure gradient located over the mountains crest east of the Greenwich meridian. West of  $0^\circ W$ , a pressure gradient is also present over the Atlas mountains, mainly controlled by the Azores anticyclone over the tropical Atlantic. The lowest pressure area is located in the Bilma erg ( $15^\circ E-15^\circ N$ ) surrounded by mountains which prevent air ventilation and allow enhanced convection inducing surface pressure low. At  $t_0+5$  (Fig. 1b), the pressure gradient over the orography east of  $0^\circ W$  has clearly increased due both to the enhancement of the high pressures in the north and to the enhancement of the heat low in the south. In particular, the 1008 hPa isoline depicts the low deepening along  $0^\circ W$ . This evolution is clearly shown by the difference field in Fig. 1c. Aside to the orography-tied dipole pressure field enhancement, we observe also a westward extension of the low pressure area over the western coast of West Africa, leading to the enhancement of westerly moist air advection from the tropical Atlantic feeding the ITCZ convection. Associated with the enhancement of the anticyclonic circulation north of the Hoggar massif, we can notice that the wind direction has changed. Just upstream of the Hoggar, the wind changed from easterly/southeasterly to easterly/northeasterly, leading from a pattern where the wind is tangential to the mountain crest line to a pattern where it flows in a more perpendicular way. Figure 1c shows that this change in direction is linked to the enhanced pressure pattern located upstream and above the Hoggar.

Figure 2 (red lines) shows the composite time series of the 1000 hPa wind direction (thin line) and speed (bold line) averaged over the area ( $10^\circ E-15^\circ E/22.5^\circ N-27.5^\circ N$ ) upstream of the Hoggar. The shift of the wind direction from  $100^\circ$  to  $80^\circ$  is very clear between  $t_0$  and  $t_0+1$ . Also, an increase of the wind speed from  $3 m s^{-1}$  to  $4 m s^{-1}$  is depicted. On the other hand, no similar signal is found at  $t_0$  upstream of the Atlas mountains and of the Ennedi, mountains (not shown) : between  $t_0-10$  and  $t_0+10$ , the 1000 hPa wind upstream of the Atlas is rather constant in direction (northwest) and no trend is evident in its strength; upstream of the Ennedi mountains, the wind speed is nearly constant with a weak variability and the wind direction is about  $35^\circ$  with a smooth decreasing trend from about  $40^\circ$  to  $30^\circ$ . Figure 2 (bold black line) also displays the difference between the mean sea level pressure over the area ( $10^\circ E-15^\circ E/22.5^\circ N-27.5^\circ N$ ) upstream of the Hoggar, and over the area ( $0^\circ W-5^\circ E/20^\circ N-25^\circ N$ ) downstream of the Hoggar. The surface pressure difference before the onset is about 2.4 hPa and sharply increases to 3.6 hPa after the onset. So the presence of the Hoggar massif seems to have an impact on the monsoon onset as the upstream wind veers from the east/southeast to the east/northeast and its speed increases from  $3 m s^{-1}$  to  $4 m s^{-1}$ , due to the anticyclonic circulation increase above and north of the Hoggar (Fig.1c). The upstream air mass thus impinges onto the Hoggar massif almost perpendicularly to the crest line.

This wind rotation as the wind speed increase are highly correlated with the pressure gradient (correlation coefficients equal respectively  $-0.79$  and  $+0.92$  over the period  $t_0-15/t_0+20$ ).

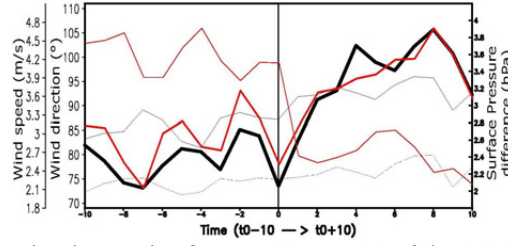


**Figure 2.** (a) Red lines : Composite time series from  $t_0-10$  to  $t_0+10$  of the 1000 hPa wind speed (bold line) and direction (thin line) averaged over the area ( $10^\circ\text{E}-15^\circ\text{E}/22.5^\circ\text{N}-27.5^\circ\text{N}$ ) upstream of the Hoggar. (b) Black lines : Composite time series of the difference between the NCEP/NCAR mean sea level pressure averaged over the area ( $10^\circ\text{E}-15^\circ\text{E}/22.5^\circ\text{N}-27.5^\circ\text{N}$ ) upstream of the Hoggar and over the area ( $0^\circ\text{W}-5^\circ\text{E}/20^\circ\text{N}-25^\circ\text{N}$ ) downstream of the Hoggar (bold line); these two boxes are displayed on Fig.1; dotted line : same as thick line but for the simulation due to the Atlas alone. Thin line : same as thick line but for the simulation due to the three massifs.

### 3. COMPARISON WITH LINEAR THEORY

In this section, linear theory is used to investigate the origin of the surface low deepening downstream the Hoggar massif at the monsoon onset. In absence of roughness effect, the surface pressure perturbation  $p_s'$  induced by the mountains on the incoming flow (with constant wind component  $U$ ,  $V$  in the  $x$  and  $y$  directions, background mean air pressure  $p$  and density  $\rho$ ) is computed from its inverse Fourier transform  $\tilde{p}$  given by the linear theory (Koffi et al. 1998):

$$\tilde{p} = i\rho \frac{N^2}{m} \tilde{h} \quad (1)$$

where  $N$  is the Brunt-Väisälä frequency,  $\tilde{h}$  the inverse Fourier transform of the orography  $h(x,y)$  and  $m$  is the vertical wavenumber given by:

$$m^2 = \left[ \frac{k^2 + l^2}{(Uk + Vl)^2 - f^2} \right] N^2 \quad (2)$$

where  $k$  and  $l$  are the wavenumbers in the  $x$  and  $y$  directions and  $f$  is the Coriolis parameter. In order to limit the number of Fourier modes and to investigate the perturbation of the flow over individual groups of mountain ranges (the Atlas, Hoggar and Ennedi mountains), the topography was smoothed and an analytical expression of each individual group of mountains was derived (see Fig.3).

Similarly to the analysis of the NCEP/NCAR composite surface pressure, the average upstream variables (surface pressure, wind speed and direction) were calculated over the area ( $10^\circ\text{E}-15^\circ\text{E}/22.5^\circ\text{N}-27.5^\circ\text{N}$ ). The average downstream variables were calculated over the area ( $0^\circ\text{W}-5^\circ\text{E}/20^\circ\text{N}-25^\circ\text{N}$ ). The inputs for the linear model, before and after the monsoon onset, are the mean wind speed and direction, the Brunt-Väisälä frequency, here assumed constant and equal to its climatological value of  $10^{-2} \text{ s}^{-1}$  and the Coriolis parameter, upstream the Atlas ridge, the Hoggar massif and the Ennedi mountains. The typical dimensionless height  $\hat{h} = Nh_0/|\mathbf{U}|$  and Rossby number  $|\mathbf{U}|/fa$  are 1.6-2 and 0.02-0.2, respectively, for our study. These high values of  $\hat{h}$  ( $>1$ ) indicate that we are pushing the small-amplitude assumption (Smith, 1982). However, because of the small Rossby number, the linear theory remains valid for higher values of  $\hat{h}$  (Ólafsson and Bougeault, 1997) and was validated against experiment during the PYREX experiment (Ólafsson and Bougeault, 1997; Bénech et al., 1998; Koffi et al., 1998).

Figure 3 shows the surface pressure perturbation before and after the monsoon onset resulting from the sum of the surface pressure perturbation computed using the linear model on each individual group of mountains. The surface pressure pattern displays similarities with the NCEP/NCAR surface pressure field shown in Fig. 1. The Atlas ridge induces a basic surface pressure low on the lee side due to the northwesterly low level flow. The surface pressure difference between the windward side and the leeward side of the Hoggar computed using the linear model is about 2.6 hPa which is in good agreement with the surface pressure difference computed using the NCEP/NCAR reanalyses (see Fig. 2). The surface pressure field from the linear model shows an increasing surface high upstream the Hoggar massif and decreasing leeward low at about  $5^\circ\text{W}$  and  $17.5^\circ\text{N}$ , which is about  $5^\circ$  latitude to the south with respect to the NCEP/NCAR surface low. The surface pressure difference computed using the linear model increases after the monsoon onset and is about 3.2 hPa

which is in good agreement with the NCEP/NCAR reanalyses (see Fig. 2). Figure 2 shows also the time series of the surface pressure difference due to the Atlas alone (dotted line), and to the three massifs (thin line). The Atlas-related gradient is rather constant and can be associated to the mean climatological signal of the Saharan heat low. The contribution of the Ennedi massif is negligible (not shown). The contribution of the three massifs is fairly similar to the observation and is in fact closely linked to the impact of the Hoggar alone.

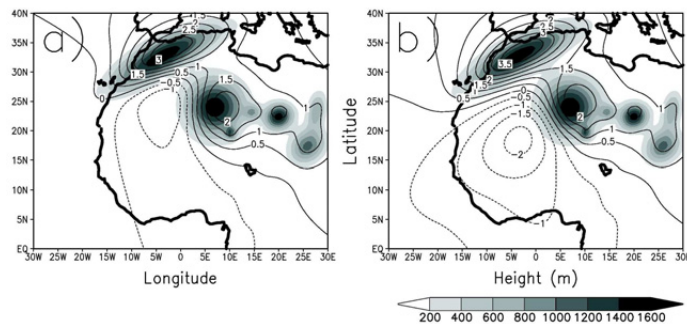


**Figure 3.** Surface pressure perturbation from the linear model (a) before the monsoon onset (similar to  $t_0-5$ ) and (b) after the monsoon onset (similar to  $t_0+5$ ). Shaded areas depict the idealized orography of northern Africa used in the linear model (m; areas higher than 400 meters are shaded by step of 100 m).

#### 4. CONCLUSION

These results confirm a possible interaction between northern Africa orography and the deepening of the Saharan heat low at the time of the monsoon onset through a positive feedback, as suggested by Sultan and Janicot (2003). However, linear models are practically limited to simple types of flow that is a small set of orography shapes (bell-shaped ridges or isolated mountains) and/or highly simplified wind profiles (constant wind, wind that varies linearly with height, wind profile with directional shear where one of the velocity components varies linearly and the other is constant). Consideration of more complicated orography shapes and/or velocity profiles requires the use of approximate methods or numerical simulations.

**Acknowledgement:** We are thankful to S. Chouarfi and M. Mellah for their help in analyzing the NCEP/NCAR reanalysis dataset; to Climate Diagnostics Center (NOAA) for providing the NCEP/NCAR Reanalysis dataset.

#### REFERENCES

- Bénech, B., E. Koffi, A. Druilhet, P. Durand, P. Bessemoulin, J. Campins, A. Jansa and B. Terliuc, 1998 : Dynamic characteristics of regional flows around the Pyrénées in view of the PYREX experiment. Part I: Analysis of the pressure and wind fields and experimental assessment of the applicability of the linear theory. *J. Appl. Meteorol.*, **37**, 32-52.
- Diedhiou, A., Janicot, S., Viltard, A., de Felice, P., and Laurent, H, 1999: Easterly wave regimes and associated convection over West Africa and the tropical Atlantic: Results from NCEP/NCAR and ECMWF reanalyses. *Climate Dyn.*, **15**, 795-822.
- Kalnay, E. et al., 1996: The NCEP/NCAR 40-year reanalysis project. *Bull. Amer. Meteorol. Soc.*, **77**, 437-471.
- Koffi, E., B. Bénech, J. Stein and B. Terliuc, 1998 : Dynamic characteristics of regional flows around the Pyrénées in view of the PYREX experiment. Part II: Solution of a linear model compared to field measurements. *J. Appl. Meteorol.*, **37**, 53-71.
- Ólafsson, H. and P. Bougeault, 1997: The effect of rotation and surface friction on orographic drag. *J. Atmos. Sci.*, **54**, 193-210.
- Smith, R.B., 1982: Synoptic observations and theory of orographically disturbed wind and pressure. *J. Atmos. Sci.*, **39**, 60-70.
- Sultan, B. and S. Janicot, 2003: The West African monsoon dynamics. Part II: The « preonset » and « onset » of the summer monsoon. *J. Climate*, **16**, 3407-3427.